특별 기고

Nanostructured Multilayer Films Based on Layer-by-Layer Assembly

Kookheon Char · Jinhan Cho

1. Introduction

Ultrathin polyelectrolyte (PE) multilayer films prepared by versatile layer-by-layer (LbL) assembly methods have been utilized for the preparation of light-emitting diodes,[1-6] electrochromic,[7,8] membrane,[9-12] and drug delivery system,[13-15] as well as for selective area patterning[16-19] and particle surface modification because various materials with specific properties can be incorporated into the films with nanometers in thickness independent of the size or shape of substrates. Since the introduction of the LbL technique in 1991 by Decher and Hong,[20] numerous polycation and polyanion pairs have been employed to form multilayer films through electrostatic interactions as schematically depicted in **Figure 1**, with strong PEs as typical components for the multilayer assembly.[21,22]

More recently, however, the assembly of films from weak PEs has attracted considerable interest because of their pH dependent characteristics.[23-28] For example, Rubner and co-workers have reported that the pH of dipping solutions has a pronounced effect on the surface roughness, film thickness, surface wettability, and the interpenetration of poly(allylamine hydrochloride) (PAH)/poly(acrylic acid, sodium salt) (PAA) multilayer films due to the change in the ionization degree of the weak PEs. They also reported that LbL SA multilayer films can be prepared based on the hydrogen-bonding interaction.[29] In 1997, Caruso and Möwhald reported that polystyrene (PS) colloidal particles can be served as a template for the build-up of PE multilayer films and, furthermore, hollow PE capsules were obtained after dissolving the PS colloids with organic solvent.[30]

In present study, we explain various interactions for the multilayer assembly and the adsorption behavior for the formation of LbL SA multilayer films and describe several examples of potential applications using such multilayered films. Furthermore, we also suggest that the modified LbL SA method based on the spin coating, replacing the conventional dipping method, could be useful for the preparation of well-defined multilayer films.

2. Intermolecular Interactions for the Formation of Multilayer Films

2.1 Multilayer Films Based on Electrostatic Interactions

차국헌

1981	서울대학교 공과대학 화학공학과 공학사
1983	한국과학기술원 화학공학과 공학석사
1989	미국 Stanford 대학교 화학공학과 공학박사(Ph.D.)
1990	미국 IBM Almaden Research Center 객원연구원
1997~1998	스위스 EPFL & 미국 코넬대학교 방문교수
2005~2006	프랑스 ESPCI & 미국 MIT 방문교수
1991~현재	서울대학교 공과대학 화학생물공학부 교수

조진한

1995	포항공과대학 화학공학과 공학사
1997	포항공과대학 화학공학과 공학석사
2001	서울대학교 화학공학과 공학박사(Ph.D.)
2001~2002	MPI Colloids & Interfaces(독일) Post-Doc.
2003	호주 Melbourne 대학교 Post-Doc.
2003~2005	LG화학 선임연구원
2006~현재	국민대학교 신소재공학과 조교수

Nanostructured Multilayer Films Based on Layer-by-Layer Assembly

서울대학교 공과대학 화학생물공학부(Kookheon Char, School of Chemical & Biological Engineering, NANO Systems Institute-National Core Research Center, Seoul National University, San 56-1, Shillim-dong, Kwanak-gu, Seoul 151-744, Korea) e-mail : khchar@plaza.snu.ac.kr

국민대학교 신소재공학과(Jinhan Cho, School of Advanced Materials Engineering, Kookmin University, 861-1, Jeongneung-dong, Seongbuk-gu, Seoul 136-702, Korea) e-mail : jinhan@kookmin.ac.kr

PEs carrying positive or negative charges are generally divided into strong and weak PEs based on the change in charge density of such PEs by pH. That is to say that strong PEs have fixed charge density irrespective of the pH change. Poly(sodium 4-styrenesulfonate) (PSS) with negatively charged SO_3^- groups and poly(diallyldimethyl-ammonium chrolide) (PDADMAC) with positively charged N^+ groups are typically classified as strong PEs. In the case of the deposition of these strong PEs onto a substrate, the electrostatic repulsion between the same charged groups causes PE chains to be adsorbed in flat and stiff chain conformation, resulting in low surface coverage and low layer thickness in the order of a few Angstroms (Å). However, the addition of ionic salt to the strong PE solutions induces the chain conformation of such PEs from flat to entangled chains due to the screening of electrostatic repulsion by counter ions and, as a result, the thickness of self-assembled layer prepared from these solutions is significantly increased (**Figure 2**).

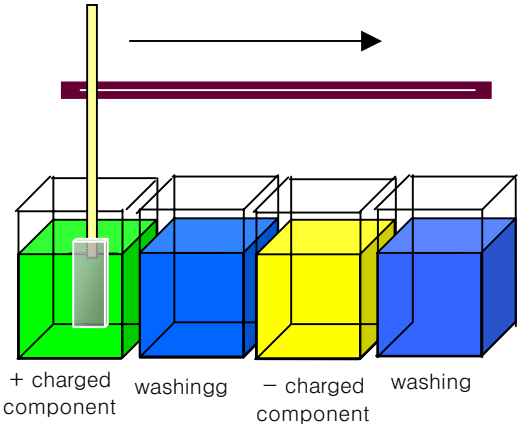

Figure 1. Schematics showing the fabrication process of PE multilayer films using electrostatic interaction.

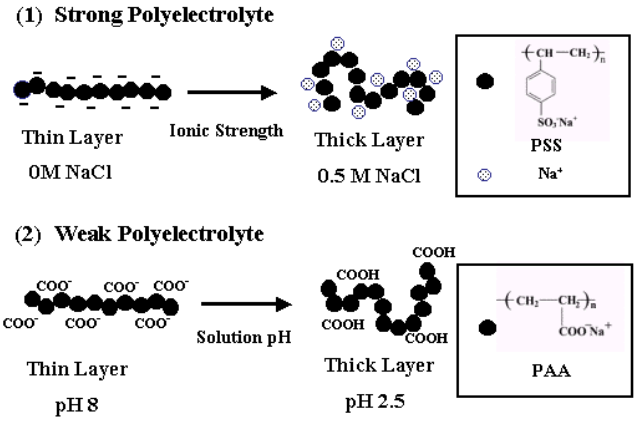

Figure 2. Schematics showing the change in chain conformation of strong and weak PEs by ionic strength and solution pH.

On the other hand, weak PEs such as poly(acrylic acid) (PAA) and poly(methacrylic acid) (PMAA) carrying carboxylic acid (COO^-) groups and PAH carrying amine (NH_3^+) groups are quite sensitive to the pH change. For example, in the case of PAA (pKa≈4.5), two different forms can coexist in PAA, enabling both electrostatic (based on $-COO^-$) and hydrogen-bonding (based on –COOH) interactions depending on pH. PAA is transformed into polyanion due to the formation of COO^- groups along the chain above pH 4.5 although PAA represents properties of neutralized polymer owing to uncharged COOH groups below pH 4.5. These changes in the charge density of weak PEs by pH have significant effects on the chain conformation of weak PEs. Therefore, with the increase in pH, the increase in the number of negatively charged groups enhances the electrostatic repulsion between adjacent COO^- groups resulting in the flat chain conformation. In contrast, the decrease in pH allows coiled PE chains because of the decrease in electrostatic repulsion, similar to the effect of ionic strength on the chain conformation for strong PEs. Rubner group reported that microporous or nanoporous PE multilayer films can be prepared through the rearrangement of adsorbed weak PE chains triggered by the pH change (**Figure 3**).[31]

2.2 Multilayer Films Based on Hydrogen-Bonding

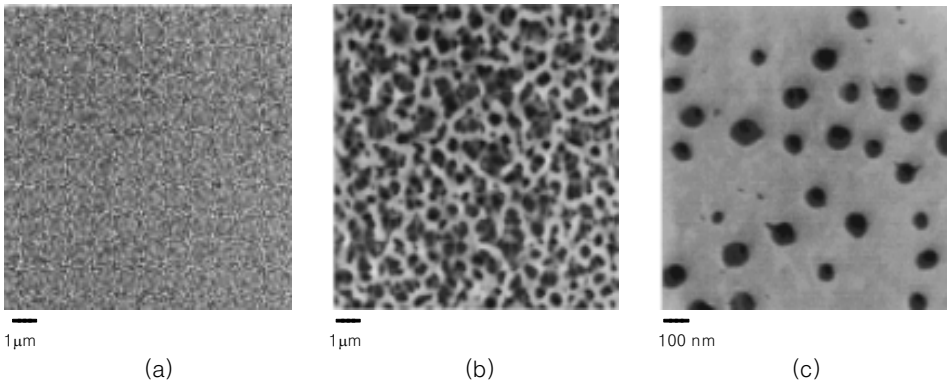

Figure 3. AFM images of the surface of a 21-layer 3.5/7.5 PE multilayer film before (a), after (b) immersion in a transition bath of pH 2.5 and then after (c) treatment in neutral water for 10 h. The film thickness and refractive index of these films are 950 Å and 1.54, 2790 Å and 1.18, and 1030 Å and 1.5, respectively.

Hydrogen-bonding (H-bonding) is regarded as a strong interaction between molecules. Although the H-bonding interaction is much weaker than the covalent bonding, multilayer films based on H-bonding pairs can also be prepared because it is still much stronger than the Van der Waals interaction.

The preparation of H-bonded multilayer films has initially been introduced by Zhang and Rubner groups.[29,32] Particularly, Zhang group demonstrated that the driving force for the formation of multilayer films composed of PAA with COOH and poly(4-vinylpyridine) (P4VP) with nitrogen atoms is the H-bonding interaction through the change of COOH (centered at 1709 cm^{-1}) and pyridine peaks (at 1556 and 1595 cm^{-1}) obtained from Fourier transform infrared spectroscopy (FT-IR).[32] Recently, Sukhishvili and Granick have reported that H-bonded multilayer films containing weak PEs, for example PAA/poly(ethylene oxide) (PEO) or poly(methacrylic acid)/poly(vinylpyrrolidone) films, could be completely degraded (or deconstructed) at pH 3.6 and 6.9, respectively.[33,34] More recently, it has been demonstrated that the H-bonded multilayer films based on PAA and poly(acryl amide) (PAAm) are highly stable at pH 7.4 after cross-linking PAA/PAAm interlayers by thermal or photoinduced treatment.[27] These findings clearly suggest the possibility of using H-bonded multilayer films based on weak PEs in applications such as micropatterning and drug delivery, where the control of the degradation rate of H-bonded multilayered films is desirable.

2.3 Covalent Bonding or Specific Interactions Involving Biomolecules

The specific binding between biomaterials such as antigen-antibody or avidin-biotin as well as the strong covalent bonding between gold nanoparticles and polymer chains containing sulfur, amine or imine moieties can also be employed for the preparation of ultrathin multilayer films.[35-37] For example, in the case of inserting the catalase for the decomposition of hydroperoxide or the urease for urea into multilayer films, the catalytic properties of enzymes within the films are maintained as they are in solution and furthermore can be improved by the control of inserted amount.[38,39] Recently, many researchers have studied these systems for the development of biosensors based on this kind of the biospecific binding.

3. Applications of Multilayer Films

3.1 Photonic Crystals

Recently, many efforts have been devoted to the photonic crystals, which are defined to have a structure with a periodic refractive index in one or higher dimensions over the length scale in the order of the wavelength of light and are typically derived from self-assembled colloids because of their relative ease of preparation and the low cost associated with their manufacture. Monodisperse colloidal spheres of silica or polystyrene are known to spontaneously self-organize into crystal structures at optical wavelength scales with long-range periodicity. Furthermore, colloidal crystals can be used as templates for fabricating 3D replicas, known as inverse opals, of metals after removing templates based on silicon or polymers.[40-42]

To date, a majority of photonic crystals prepared from colloidal particles have employed commercially available colloids, such as silica or polystyrene spheres. Utilization of composite colloids, particularly, core-shell or coated particles, represents an interesting alternative to the realization of novel photonic crystals. Recently, Caruso group reported the fabrication and optical properties of metallodielectric crystals derived from (gold/PE)-coated colloids prepared by the LbL approach as depicted in **Figure 4**.[43]

On the other hand, Rubner group reported 1D photonic crystals formed by alternatively depositing respective multilayer strata with high and low refractive indices.[44] They have previously demonstrated that the PAH/PAA multilayers could be served as a template within which inorganic nanoparticles could be synthesized. Carboxylic acid groups in the PAH/PAA multilayers strongly bind to metal cations from aqueous solution via the ion exchange. Upon the reduction of metal cations within the multilayers, zero-valence metal nanoparticles are formed. This *in-situ* synthetic approach facilitates the preparation of controlled concentration of homogeneously dispersed nanoparticles throughout

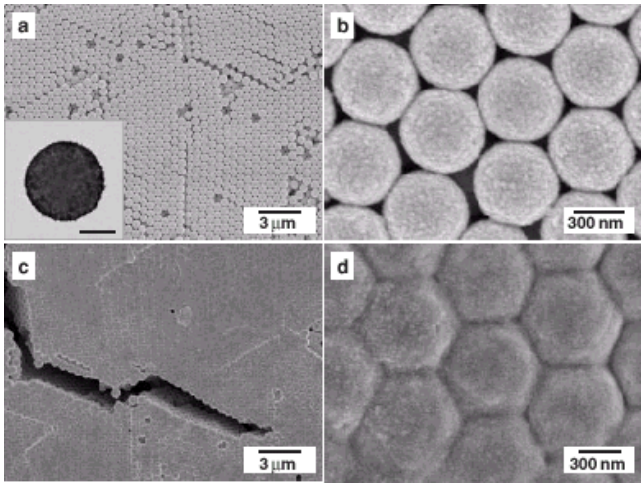

Figure 4. SEM images of crystalline arrays of PS spheres coated with $(PAH/PSS)_2$/Au/PEI/PSS (a, b) and PS-$(PAH/PSS)_4$/PEO opal templates infiltrated with Au (c, d). The inset in (a) shows a TEM image of a PS sphere coated with (PAH/PSS)2/Au/PEI/PSS, displaying the uniformity of the 6 nm diameter Au coating. The scale bar in the inset corresponds to 300 nm.

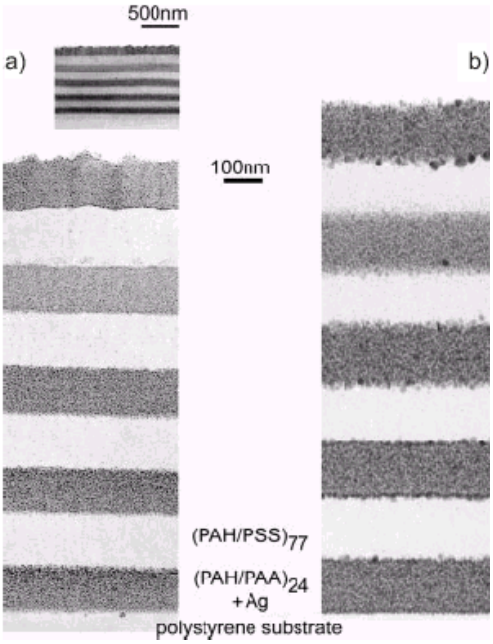

Figure 5. Cross sectional TEM images of a 4.5 period Bragg stack after (a) one cycle of Ag nanoparticles synthesis and (b) five cycles of nanoparticles synthesis. In (a), the high index strata (dark contrast) have average thicknesses of 120±4 nm and the low index strata (light contrast) have average thicknesses of 137±6 nm. In (b), after five cycles of nanoparticles synthesis, the average thicknesses of high index stratum is 167±7 nm (containing~19 vol% Ag) and of the low index stratum is 148±9 nm.

the multilayer and can be repeatedly cycled to increase the metal (for example, silver) volume fraction. Therefore, after the preparation of multilayer films composed of $(PAH/PAA)_n$ and $(PAH/PSS)_n$, the dipping of the films into silver acetate solution yields a nice Bragg diffraction consisting of high refractive index strata with silver nanoparticles and low refractive index strata without nanoparticles (**Figure 5**).

3.2 Biocolloids for Drug Delivery Systems

Novel hollow microcapsules with size ranging from 60 nm to 10 μm have recently been produced by the LbL assembly of oppositely charged PEs onto colloidal templates, followed by the removal of the template cores.[14-16] In this case, specific chemical compounds typically with low molecular weight can be inserted into or be released from the PE microcapsules by the change in physical or chemical properties of the PE multilayers which are highly dependent on ionic strength, solution pH, and electrostatic interaction. Gao *et al.* have reported the preparation of PE microcapsules using melamine formaldehyde (MF) colloids as a template and the spontaneous entrapment of low molecular weight compounds within the interior of microcapsules, as shown in **Figure 6**.[45] It should be noted here that a substance can spontaneously diffuse from a low concentration region to a high concentration region of the capsule suspension system with the enthalpic electrostatic interaction. They postulated

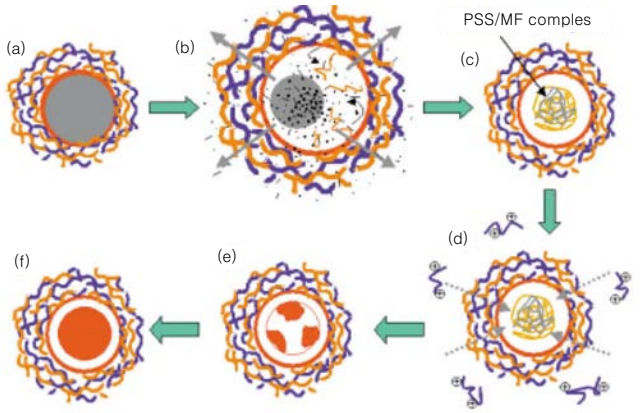

Figure 6. Schematic illustration of spontaneous deposition mechanism based on the formation of the PSS/MF complex during the core decomposition process.

that the driving force for the diffusion originates from the charged species already existing within the interior of intact capsules. More specifically, upon subjecting the PE-coated MF particles (a) to lower pH conditions (i.e., 0.1 M HCl), the core material, a slightly cross-linked MF resin, degrades into small particles and diffuses out of the capsule wall at the same time, while the capsule itself increases its size due to the osmotic difference (b) (**Figure 6**). While this process occurs, the first layer (PSS) is partially detached from the capsule wall and migrates into the interior of the capsule to form a complex with residual positively charged MF core particles. The complex formed within the core is too large to diffuse out of the intact capsule wall (c). The net charge of the PSS/MF complexes is negative (as evidenced from the zeta potential measurements) and the existence of the PSS/MF complexes provides an additional driving force to attract water-soluble substances within the capsule core, particularly positively charged moieties, and to deposit around the complexes (d, e), thus promoting the self-deposition (f).

Caruso *et al.* reported that an enzyme crystal (catalase), which has biocatalytic property to dissociate H_2O_2 gas, can also be used as a template for PE multilayers instead of colloidal silica, PS or MF because the catalase exists as a positively charged crystal when the solution is between pH 5 and 6.[46] They also demonstrated that biosensors prepared from the PE-coated catalases could significantly improve the sensitivity compared with conventional biosensors. On the other hand, the release of catalase from the PE microcapsules is induced from the catalase solubilization as well as PE decomposition by the pH adjustment as schematically represented in **Figure 7**.

It is also well known that a number of biomaterials have zwitterionic characteristics due to the co-existence of car-

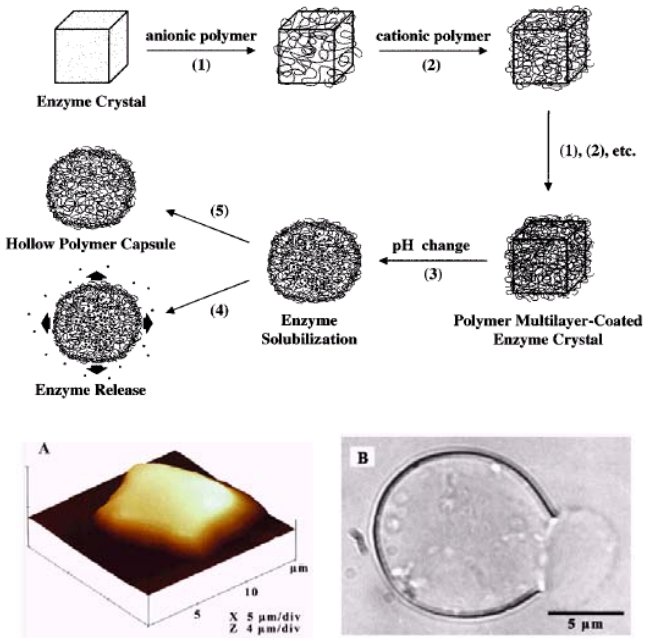

Figure 7. Schematics showing the process used to encapsulate enzymes by using biocrystals as templates for the deposition of polymer multilayers, subsequent enzyme solubilization and release, and the formation of hollow polymer capsules. (1, 2) PE layers are deposited stepwise onto the crystals by making use of the surface charge reversal that occurs upon adsorption of each layer. Each PE layer deposited bears an opposite charge to that already adsorbed. Weakly adsorbed PEs are removed by repeated centrifugation/wash redispersion cycles before the next layer is deposited. (3) Solubilization of the enzyme inside polymer capsule by exposure. (A) Tapping mode AFM images of enzyme crystals and (B) Rupturing of a polymer multilayer capsule causes the release of the entrapped, solubilized enzyme. Rupturing is achieved by subjecting the polymer capsules to alkaline solutions of pH > 11.

boxylic acid and amine groups. Therefore, various biomaterials can be incorporated into ultrathin multilayer films through the electrostatic intermolecular interactions and as a result, biosensors with specific functions can be easily fabricated.

3.3 Anti-reflection Film

Anti-reflection coatings play an important role in a wide variety of optical technologies by reducing reflective losses at the interfaces. Optical elements based on glasses and common plastics have refraction indices (n) in the range of 1.45~1.7 and, as a result, reflect from 4% to more than 6.5% of normal incident light from any single air-substrate interface.[47] In applications such as flat-panel displays, anti-reflection coatings are typically employed to eliminate the effects so-called 'ghost images', or veil glares originating from stray and multiple reflections from the optical surfaces. Reflection losses from optical components are also notably undesirable in technologies such as solar cell collectors, which rely on efficiently transmitted energy. It is therefore necessary to reduce the intensity of reflected light to improve the overall quality, performance and efficiency of such optical systems, which translates to increasing transmission, improving contrast and reducing glare, as well as eliminating ghost images.

A reduction in surface reflection can be typically accomplished by satisfying two requirements as follows :

$$n_f \approx (n_{sub} \times n_{air})^{0.5} \quad (1)$$

$$T_f \approx \lambda / (4 n_f) \quad (2)$$

where n_f, n_{sub} and n_{air} are the refractive index of film, substrate and air, respectively. Consequently, the refractive index and the thickness of ideal anti-reflective film should be about 1.22 and be between 100 and 160 nm, respectively if anti-reflective film is coated onto glass substrate ($n \approx 1.50$). However, almost all the coating materials have a difficulty in achieving the refractive index of 1.22 without introduction of homogeneous nanopores within the films.

Recently, we reported the antireflective block copolymer micelle/micelle multilayer films prepared through the fine tuning of the solution pH, molecular weight (M_w) of micelles and film thickness.[48] Protonated polystyrene-*block*-poly(4-vinylpyridine) (PS-*b*-P4VP) and anionic polystyrene-*block*-poly(acrylic acid) (PS-*b*-PAA) block copolymer micelles (BCM) were used as building blocks for the layer-by-layer assembly of BCM multilayer films. BCM film growth is governed by electrostatic and hydrogen-bonding interactions between the oppositely BCMs. Both film porosity and film thickness are dependent upon the charge density of the micelles, with the porosity of the film controlled by the solution pH and M_w of the constituents. $PS_{Mw\sim 7K}$-*b*-$P4VP_{Mw\sim 28K}$/PS_{2K}-*b*-PAA_{8K} films prepared at pH 4 (for PS_{7K}-*b*-$P4VP_{28K}$) and pH 6 (for PS_{2K}-*b*-PAA_{8K}) are highly nanoporous and antireflective. In contrast, PS_{7K}-*b*-$P4VP_{28K}$/PS_{2K}-*b*-PAA_{8K} films assembled at pH 4/4 show a relatively dense surface morphology due to the decreased charge density of PS_{2K}-*b*-PAA_{8K}. Films formed from BCMs with increased PS block and decreased hydrophilic block (P4VP or PAA) size (e.g., PS_{36K}-*b*-$P4VP_{12K}$/PS_{16K}-*b*-PAA_{4K} at pH 4/4) were also nanoporous. This is attributed to a decrease in interdigitation between the adjacent corona shells of the low M_w BCMs, thus creating more void space between the micelles. **Figure 8(a)** and **(b)** show the surface morphology of (pH4 PS_{7K}-*b*-$P4VP_{28K}$/pH6 PS_{2K}-*b*-PAA_{8K})$_{30}$ and the light transmission of PS-*b*-P4VP/PS-*b*-PAA multilayer films with various M_w.

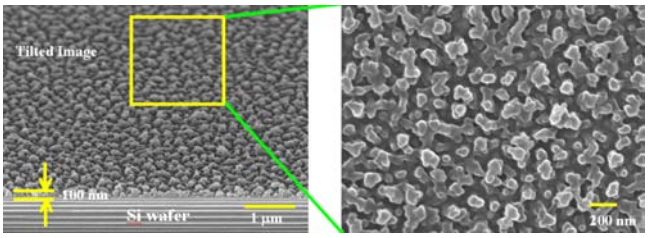

(a)

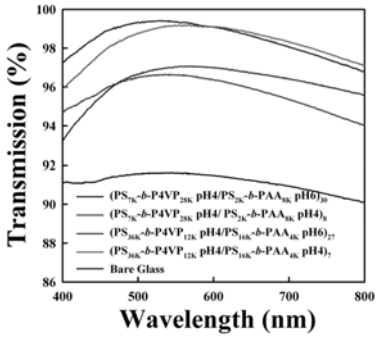

(b)

Figure 8. (a) SEM images of nanoporous $(PS_{7K}-b-P4VP_{28K}/PS_{2K}-b-PAA_{8K})_{30}$ multilayer films formed at pH4/6. (b) Light transmission curves of (a) $(PS_{7K}-b-P4VP_{28K}/PS_{2K}-b-PAA_{8K})_n$ and $(PS_{36K}-b-P4VP_{12K}/PS_{16K}-b-PAA_{4K})_n$ multilayer films assembled at different pH.

4. Ultrathin Multilayer Films Using Spin-Assembly Method

4.1 Fabrication and Characteristics of Films

Although the LbL assembly method is powerful method for fabricating the ultrathin multilayer films composed of cationic and anionic PEs, this LbL method is principally based on the self-diffusion process in which charged PE chains are adsorbed onto an oppositely charged surface due to the electrostatic attraction. As a result, the adsorption time, proper control of pH, PE concentration and the amount of added ionic salt should be considered in order to increase the surface coverage of a polymer layer adsorbing onto a substrate. In addition, without thorough washing using a flow of pure solvent after the adsorption of a polyelectrolyte layer, the weakly adsorbed PE chains significantly increase the surface roughness of the multilayer films, yielding poor film quality. Consequently, optimum conditions for both adsorption and careful washing steps are required in order to prepare well-defined multilayer films.

Recently, we have reported a spin-assembly method using a spinning process as an alternative to fabricate well-organized multilayer films in a very short process time.[49] PAH and PSS were, for example, used as a cationic and an anionic polymer, respectively. Inorganic cadmium sulfide (CdS) nanoparticles carrying negative charges at the particle surface were also employed in order to demonstrate the quality of the internal structure of multilayer films prepared by the spin assembly method.

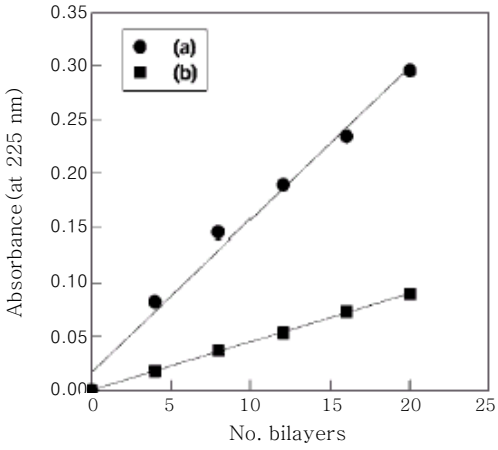

Figure 9. Absorbance at 225 nm of PAH/PSS multilayers prepared by (a) spin-assembly method and by (b) dip SA method.

Figure 9 shows the difference in UV/vis absorbance of multilayer films with alternating PAH and PSS layers prepared by both spin SA and dipping SA methods. The aqueous PE concentrations of PAH and PSS used in the two different deposition methods were all identical to be 10 mM. At each deposition step, the spin SA process was performed at a spinning speed of 4,000 revolutions per minute (rpm) and then twice the washing steps with pure deionized water at the same spinning speed. On the other hand, the dipping process was performed for an adsorption time of 20 min per layer in order to allow enough time for the saturated adsorption. The absorbance at 225 nm in the UV region was assigned to be the contribution from the adsorbed PSS chains. It should be noted at this point that the multilayer film fabricated by the spin assemly method is adsorbed onto only one side of a quartz wafer while the film prepared by the dipping assembly method is adsorbed onto both sides of a quartz wafer. The film thickness per bilayer adsorbed by both the spinning process and the dipping process was found to be about 24 Å and 4 Å, respectively, as determined from ellipsometric measurement when the same mole concentrations of the PEs were used.

This significant difference in the adsorbed amount between the dipping and the spinning method is caused by different adsorption mechanism. In the case of the conventional assembly method by the dipping process, PE chains are allowed to diffuse toward the substrate due to the electrostatic interaction and then the adsorbed chains rearrange themselves on the surface. On the other hand, the adsorption and rearrangement of adsorbed chains on the surface and the elimination of weakly bound polymer chains from the substrate in the spin assembly process

are almost simultaneously achieved by a high spinning speed for a short time. Fast elimination rate of water by the spinning process significantly increases the mole concentration of the PE solution during the short deposition time and this increase in the PE concentration yields thick layers despite the thin film formation typically provided by the centrifugal force and air shear force.[50-52] It also increases the electrostatic attraction between oppositely charged polymers because the presence of water molecules in the assemblies generally screens the electrostatic attraction. In other words, when water molecules are adsorbed onto a substrate, the preadsorbed water molecules may block the PE adsorption onto the surface, and thus the surface coverage with PE chains may be incomplete. However, if polymer adsorption and water drainage are almost simultaneously realized in a short time, as in the case of the spinning self-assembly process, there would be more room for PEs to adsorb onto the substrate. **Figure 10** schematically represents these driving forces caused by the spinning process.

Figure 11 shows the change in water contact angles of dip and spin SA $(PAH/PSS)_n$ films when the outermost layer is alternatively changed from PAH to PSS or from PSS to PAH. Odd and even numbers represent the top surface layers of PAH and PSS, respectively. First, in the case of the dip SA film repeatedly deposited from PE solutions of 10 mM without the addition of ionic salt, all the contact angles measured on PAH and PSS except the first two layers are within the range of 25~28° without evident

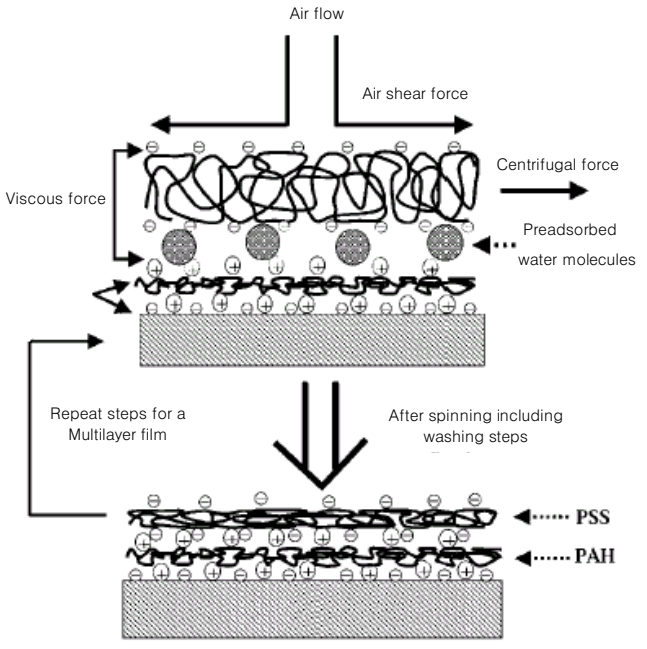

Figure 10. A side view schematic depicting the build-up of multilayer assemblies by consecutive spinning process of anionic and cationic PEs.

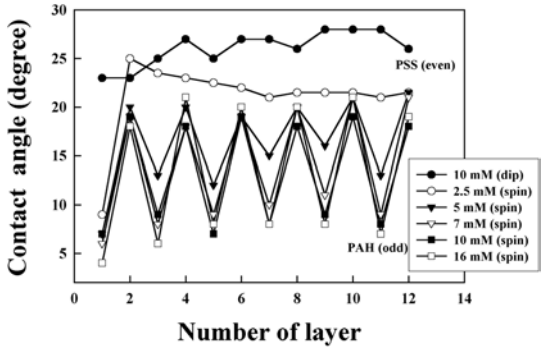

Figure 11. Water contact angles measured from PAH/PSS multilayers prepared with dip SA and spin-assembly methods. Odd and even numbers indicate the layers deposited with PAH and PSS, respectively.

periodic oscillation. This disappearance of oscillatory trend of the contact angles obtained from our experimental conditions reflects that the respective layers form rather disordered layers (i.e., mixed layers) composed of interdigitated PAH and PSS segments owing to the insufficient surface coverage as well as the high surface roughness of 8 Å compared with the bilayer thickness of 4 Å.[53] In contrast, for the spin SA multilayer films deposited from the five different mole concentrations of PE solutions, the increase in PE concentration significantly increases the oscillation behavior of the contact angles up to about 7 mM and then levels off at higher concentration. The contact angles of the PAH and PSS top layers are also found to be quite low in comparison with those of dip SA films. However, for the spin SA films prepared with a PE concentration of 2.5 mM, it is assumed that the PAH layer with 3 Å thickness and the PSS layer with 5 Å thickness, carrying a surface roughness of about 2~3 Å, do not establish the well-ordered laminate structure because of insufficient surface coverage as mentioned above. This assumption is supported by the fact that the contact angles obtained from a PE concentration of 2.5 mM indicate no periodic oscillations when the outermost layers are alternately changed. On the other hand, the relatively thick outermost layers prepared by PE concentrations above 7 mM, fully covering the surface roughness of the sublayer, yields distinct and periodic oscillations of the contact angles. It is additionally pointed out that the spin SA outermost layers (i.e., PAH and PSS) with the PE concentrations of 7, 10 and 16 mM demonstrate the similar contact angles despite of the increase in individual layer thickness. These similarities can be explained in light of physical and chemical characteristics. That is to say that the formation of the top surface layers with sufficient surface coverage as well as extremely smooth surface significantly contributes to the screening surface effects of the sublayer, decreasing the

length scale of interdigitated layer that can share the chemical properties of PAH and PSS.

In order to confirm our hypothesis described above, we prepared negatively charged CdS nanoparticles with a diameter of about 2 nm and then investigated the internal structure of $[(PAH/PSS)_n/(PAH/CdS)_1]_m$ ($[n+1]\times m=20$ or 21) multilayer films exploiting the significant electron density difference between a polyelectrolyte layer and an inorganic nanoparticle layer. As shown in **Figure 12**, all the multilayer films, with different numbers of the (PAH/ PSS) bilayer in each repeat organic/inorganic layer ranging from 0 to 4, clearly exhibit the Bragg reflection peaks originating from the internal structure. The surface roughness of the five different multilayer films measured from AFM is about 5 Å. It is particularly striking to note that the existence of Bragg peak even in the $(PAH/CdS)_{20}$ film composed of alternating a nanoparticle layer of 20 Å in diameter and a PAH layer of 6 Å in thickness strongly indicates that each layer in the multilayer films forms an almost perfect superlattice layer carrying a sharp internal interface in spite of the ultrathin film of the organic layer.

However, in the case of a $(PAH/CdS)_{20}$ multilayer film prepared by the conventional SA method, the average bilayer thickness is about 6 Å and this bilayer thickness is yet much smaller than the average CdS nanoparticle size of 20 Å. In addition, the surface roughness of the film is found to be around 18 Å. This disagreement between the bilayer thickness and the nanoparticle size for a film prepared by the dipping method is believed to be caused by the insufficient surface coverage of respective layers and this further causes less electron density difference between organic and inorganic layer, as mentioned in several papers.[54-56] This distinct difference in the dipping and the spin SA multilayer structures clearly indicates that the spin SA method can easily provide the well-ordered internal structure which cannot be achieved with the dipping SA even containing high ionic strength of the PE solution or multiple organic layers between inorganic particle layers.

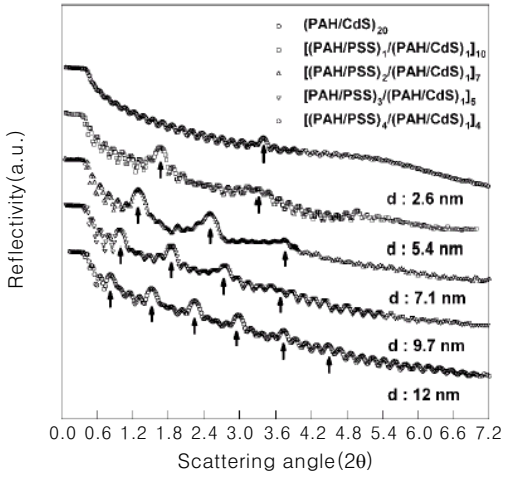

Figure 12. X-ray reflectivity curves of $[(PAH/PSS)_n/(PAH/CdS)1]_m$ ($[n+1]\times m=20$ or 21) films prepared with spin SA method. The increase of bilayer number of (PAH/PSS) from 0 to 4 causes the increase of d-spacing between polyelectrolyte and nanoparticles from 2.6 to 12 nm. The arrow symbols in the figure indicate Bragg peaks of such an internal structure.

4.2 Patterned Multilayer Films

It has been reported that dip SA multilayer patterns can be easily fabricated using micro-contact printing.[17-20] However, the spin SA method has difficulty in preparing the multilayer films selectively adsorbed onto chemically patterned substrates using the microcontact printing method because the adsorption selectivity for patterning significantly decreases, due to the memory effect of PE chains loosely adsorbed onto unpatterned area, with increasing the number of PE layers. As an alternative, we have recently reported the patterning technique using the spin assembly in microfluidic channels.[57] As shown in **Figure 13**, PDMS mold carrying the microfluidic channels is placed onto the flat substrate and then, the alternate deposition of each other different materials yields the multilayer pattern after spinning process. Although this method provides the inherent selective adsorption control owing to the use of the microfluidic channels, it is generally limited to line patterns

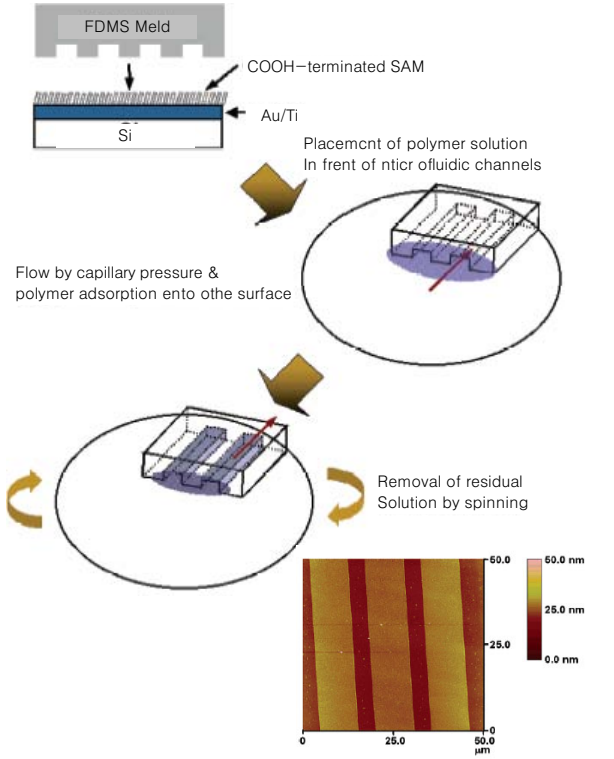

Figure 13. Schematic micropatterning and AFM image of multilayer films using the convective-assembly process.

because of the directionality of a driving force (i.e., centrifugal force) during the spinning process.

As an alternative, patterned multilayer films are fabricated in a very short time using the combination of spin self-assembly and lift-off method as show in **Figure 14**. First, a photoresist thin film deposited onto a silicon substrate was patterned from conventional photolithography and then PAH/PSS multilayers prepared by spin assembly method were uniformly coated onto the whole area of substrate.[58] In this case, it is observed that the photoresist structure onto substrate is not destroyed despite the high centrifugal force for PE deposition process. For the preparation of patterned multilayer films, the PE coated substrate are immersed into acetone solvent for about 10 min,

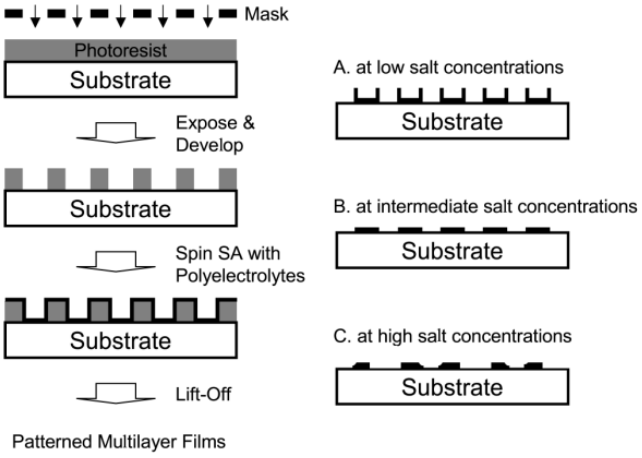

Figure 14. Patterning procedure of multilayer films based on spin SA and lift-off method and change in pattern formation (A~C) by ionic strength.

accompanying the removal of both the patterned photoresist and the PE layers deposited onto it.

Figure 15 shows that the pattern quality such as line-edge definition is significantly dependent on the ionic salt concentration added into the PE solutions.[58] In the case of PAH/PSS multilayer films prepared without any salt, the relatively high edge profile indicates that a large amount of PAH/PSS layers formed onto a photoresist is not completely removed and an edge pattern on both sides of a line is instead formed even after the lift-off of the photoresist. In contrast, in the case of PAH/PSS multilayers deposited with high ionic strength, the lift-off process removes even the multilayer films adsorbed onto the substrate without a photoresist as well as patterned photoresists since the multilayers presumably carry weakly bound PE chains. Based on the two extreme cases that depend on the ionic strength, it is expected that the spin SA layers deposited on the photoresist can be completely removed without damaging the PE multilayers on a desired film pattern area at an intermediate ionic strength. As shown in **Figure 15(b)**, the optimum electrolyte (NaCl concentration of 0.4 M) used in our system provides a well-defined multilayer pattern achieving a low edge height of 10 nm with a root mean square (rms) surface roughness of 3 nm.

Furthermore, the well-defined patterns of organic/inorganic multilayer films consisting of PE and gold nanoparticles of about 6 nm in size are simply prepared using the spin assembly & lift-off method as shown in **Figure 16**.

4.3 Organic/Inorganic Multilayer Composites

The material of seashell nacre and bones are well known for their hardness, strength and thoughness,

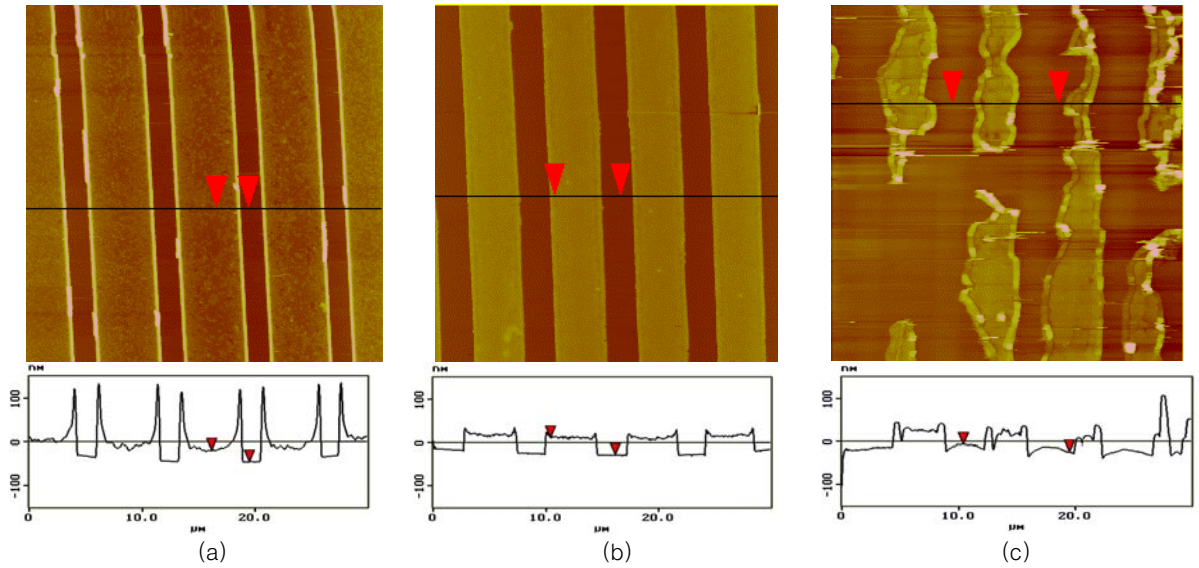

Figure 15. AFM images of the patterned multilayer films of $(PAH/PSS)_{20}$ prepared in different deposition solutions: (a) no salt solution, (b) 0.1 M NaCl solution, (c) 0.4 M NaCl solutions, and (d) 1.0 M NaCl solution.

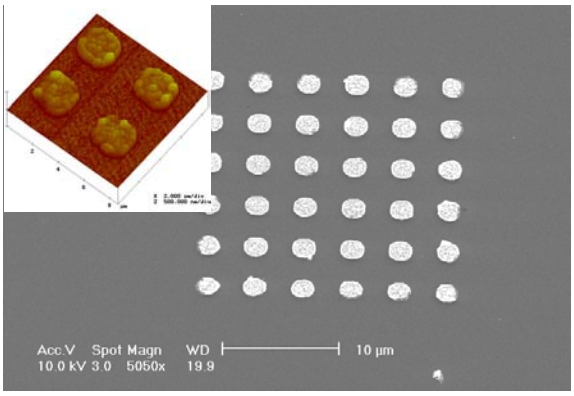

(a)

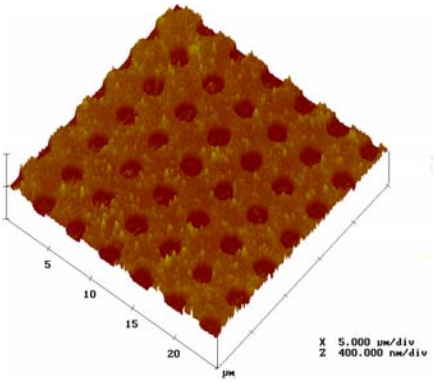

(b)

Figure 16. (a) SEM and (b) AFM images of patterned $[(PAH/PSS)_3 Au/PSS]_3$ film.

superior to man-made ceramics and composites, complemented by unique biological/biomedical properties.[59-61] Their distinctive mechanical qualities are attributed to a highly regular brick and mortar arrangement of organic and inorganic elements, which combines the elasticity of 10 ~ 50 nm protein layers (for example, β-chitin and lustrins) and the strength of $CaCO_3$ tablets 200~900 nm thick.[59] The structure-function harmony of nacre and other hard biological tissues has inspired a large class of bimimetic advanced materials and organic/inorganic composites. The addition of inorganic components, such as clays, to organic polymers noticeably improves the mechanical, barrier and thermal properties of polymers and mechanical characteristics similar to nacre have yet to be made. Besides the ordered layered structure, nacre mimics should also display interfacial compatibility of organic and inorganic parts, as well as tight folding of the polymer chains resulting in sacrificial ionic bonds. The tight polymer folding is responsible for the inelastic behavior of nacre that is crucial for notch resistance and an exceptionally high amount of energy that hard biological tissues can absorb. Recently, we reported that organic PE/inorganic silicate nanolaminates carrying strong electrostatic adhesion between the

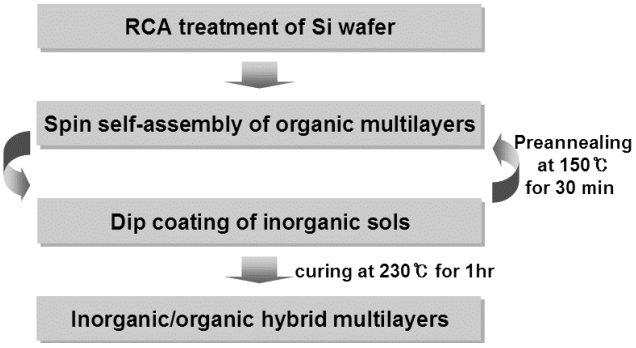

Figure 17. A schematic depicting the build-up of organic/inorganic hybrid nanolaminates.

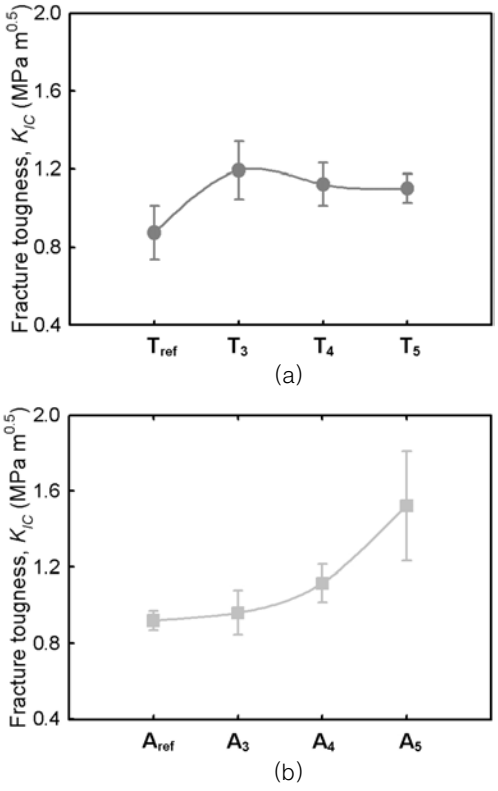

Figure 18. Change in fracture toughness with the increase in PE thickness in each organic layer for (a) T_n series and (b) A_n series with n=0, 3, 4, and 5.

organic and the inorganic layers could significantly improve the mechanical strength in comparison with those prepared using only van der Waals interaction between organic and inorganic layers.[62] For this investigation, organic/inorganic multilayer films were prepared with (organo)silicate oligomers (precursors) as an inorganic layer in combination with PE multilayers as an organic layer. While the inorganic precursor is deposited by dip coating, the PE organic multilayers are deposited onto a substrate by the spin SA method. This combination of dip coating and spin SA method allows us to prepare hybrid multilayer films with relatively thick inorganic layers as well as with highly ordered internal

structure. In present case, the electrostatic interaction between PE and silicate layers as well as between adjacent PE layers was employed in varying degree for the build-up of hybrid multilayer films. In order to investigate the effect of interfacial adhesion between the PE and the silicate layers on the fracture toughness more specifically, two different kinds of films were prepared as follows: T_n series with weak electrostatic interaction between PE and silicate layers and A_n series with relatively strong electrostatic interaction compared with the T_n series.[63]

In order to investigate the mechanical behavior of the prepared hybrid films, the fracture toughness of the hybrid films was then calculated using the measured mechanical values such as apparent modulus, hardness and crack length. In the case of forming a strong interfacial adhesion between the organic and the inorganic layers (A-series), the fracture toughness and the crack resistance of hybrid multilayer films were significantly improved due to the redistribution of stress concentration and the dissipation of fracture energy by the plasticity of organic PE layers. On the other hand, samples with relatively low interfacial adhesion between the organic and the inorganic layers (T-series) had little effect on the improvement of fracture toughness of the hybrid films.

5. Summary

We described the various interactions for the formation of LbL multilayer films, the adsorption behavior of PEs and the potential possibilities applicable to optical device, display or drug delivery system. Furthermore, it was demonstrated that the spin assembly process utilizing centrifugal force, viscous force, air shear and electrostatic interactions causes the adsorption, the rearrangement of polymer chains onto a substrate and the desorption of weakly bound chains in a very short time of approximately 10 seconds. This new ultrathin film-forming process, despite much simpler and faster in comparison with the conventional dipping assembly process, yields a highly ordered internal structure far superior to the structure obtained with the dipping assembly process. It was also suggested that micropatterns with various shapes can be fabricated using spin assembly process which precisely controls and predicts the bilayer thickness as well as the surface roughness.

Acknowledgements : JC acknowledges the financial supports from the New Faculty Research Program 2006 at Kookmin University in Korea as well as from the SRC/ERC Program of the MOST/KOSEF (R11-2005-048-00000-0). KC also acknowledges the financial support from the NANO Systems Institute-National Core Research Center from the Korea Science and Engineering Foundation (KOSEF).

References

1. P. K. H. Ho, J.-S. Kim, J. H. Burroughs, H. Becker, S. F. Y. Li, T. M. Brown, F. Cacialli, and R. H. Friend, *Nature*, **404**, 481 (2000).
2. P. K. H. Ho, M. Granstrom, R. H. Friend, and N. C. Greenham, *Adv. Mater.*, **10**, 769 (1998).
3. A. C. Fou, O. Onitsuka, M. Ferreira, M. F. Rubner, and B. R. Hsieh, *J. Appl. Phys.*, **79**, 7501 (1996).
4. O. Onitsuka, A. C. Fou, M. Ferreira, B. R. Hsieh, and M. F. Rubner, *J. Appl. Phys.*, **80**, 4067 (1996).
5. M. Eckle and G. Decher, *Nano Lett.,* 1, 45 (2001).
6. J. Cho, K. Char, S.-Y. Kim, J.-D. Hong, S. K. Lee, and D. Y. Kim, *Thin Solid Films*, **379**, 188 (2000).
7. D. M. DeLongchamp and P. T. Hammond, *Chem. Mater.*, **16**, 4799 (2004).
8. D. M. DeLongchamp and P. T. Hammond, *Adv. Mater.,* **13**, 1455 (2001).
9. D. M. Sullivan and M. L. Bruening, *J. Am. Chem. Soc.*, **123**, 11805 (2001).
10. S. T. Dubas, T. R. Farhat, and J. B. Schlenoff, *J. Am. Chem. Soc.*, **123**, 5368 (2001).
11. H. H. Rmaile and J. B. Schlenoff, *J. Am. Chem. Soc.*, **125**, 6602 (2003).
12. B. W. Stanton, J. J. Harris, M. D. Miller, and M. L. Bruening, *Langmuir*, **19**, 7038 (2003).
13. F. Caruso, R. A. Caruso, and H. Möhwald, *Science*, **282**, 1111 (1998).
14. G. Ibarz, L. Dähne, E. Donath, and H. Möhwald, *Adv. Mater.,* **13**, 1324 (2001).
15. Z. Dai, A. Voigt, S. Leporatti, E. Donath, L. Dähne, and H. Möhwald, *Adv. Mater.*, **13**, 1339 (2001).
16. S. L. Clark, M. F. Montague, and P. T. Hammond, *Macromolecules*, **30**, 7237 (1997).
17. S. L. Clark and P. T. Hammond, *Adv. Mater.*, **10**, 1515 (1998).
18. S. L. Clark, E. S. Handy, M. F. Rubner, and P. T. Hammond, *Adv. Mater.*, **11**, 1031 (1999).
19. I. Lee, H. Zheng, M. F. Rubner, and P. T. Hammond, *Adv. Mater.*, **14**, 572 (2002).
20. G. Decher, J.-D. Hong, and J. Schmitt, *Macromol. Chem., Macromol. Symp.*, **46**, 321 (1991).
21. G. Decher, J.-D. Hong, and J. Schmitt, *Thin Solid Films,* **210**, 831 (1992).
22. G. Decher, *Science*, **277**, 1232 (1997).
23. D. Yoo, S. S. Shiratori, and M. F. Rubner, *Macromolecules,* **31**, 4309 (1998).
24. S. S. Shiratori and M. F. Rubner, *Macromolecules,* **33**, 4213 (2000).
25. J. D. Mendelsohn, C. J. Barrett, V. V. Chan, A. J. Pal, A. M.

Mayes, and M. F. Rubner, *Langmuir*, **16**, 5017 (2000).
26. T. C. Wang, M. F. Rubner, and R. E. Cohen, *Langmuir*, **18**, 3370 (2002).
27. S. Y. Yang and M. F. Rubner, *J. Am. Chem. Soc*., **124**, 2100 (2002).
28. J. Cho and F. Caruso, *J. Am. Chem. Soc.,* **126**, 2270 (2004).
29. W. B. Stockton and M. F. Rubner, *Macromolecules*, **30**, 2717 (1997).
30. F. Caruso, R. A. Caruso, and H. Möhwald, *Science*, **282**, 1111 (1998).
31. J. D. Mendelsohn, C. J. Barrett, V. V. Chan, A. J. Pal, A. M. Mayes, and M. F. Rubner, *Langmuir*, **16**, 5017 (2000).
32. L. Wang, Y. Fu, Z. Wang, Y. Fan, and X. Zhang, *Langmuir*, **15**, 1360 (1999).
33. S. A. Sukhishvili and S. Granick, *J. Am. Chem. Soc.,* **122**, 9550 (2000).
34. S. A. Sukhishvili and S. Granick, *Macromolecules*, **35**, 301 (2002).
35. J. Anjai, H. Takeshita, Y. Kobayashi, T. Osa, and T. Hoshi, *Anal. Chem*., **70**, 811 (1998).
36. T. Hoshi, J. Anjai, and T. Osa, *Anal. Chem*., **34**, 770 (1995).
37. J. F. Hicks, Y. Seok-Shon, and R. W. Murray, *Langmuir*, **18**, 2288 (2002).
38. M. Onda, Y. Lvov, K. Ariga, and T. Kunitake, *Biotechnol. Bioeng*., **51**, 163 (1996).
39. F. Caruso, K. Niikura, D. N. Furlong, and Y. Okahata, *Langmuir*, **13**, 3427 (1997).
40. O. D. Veleve and E. W. Kaler, *Adv. Mater*., **12**, 531 (2000).
41. Y. Xia, B. Gates, Y. Yin, and Y. Liu, *Adv. Mater.,* **12**, 693 (2000).
42. K. M. Kulinowski, P. Jiang, H. Vaswani, and V. L. Colvin, *Adv. Mater.,* **12**, 833 (2000).
43. Z. Liang, A. S. Susha, and F. Caruso, *Adv. Mater*., **14**, 1160 (2002).
44. T. C. Wang, R. E. Cohen, and M. F. Rubner, *Adv. Mater*., **14**, 1534 (2002).
45. C. Gao, E. Donath, H. Möhwald, and J. Shen, *Angew. Chem. Int. Ed*., **41**, 3789 (2002).
46. F. Caruso, D. Trau, , H. Möhwald, and R. Renneberg, *Langmuir*, **16**, 1485 (2000).
47. J. Hiller, J. D. Mendelsohn, and M. F. Rubner, *Nature Materials*, **1**, 59 (2002).
48. J. Cho, J. Hong, K. Char, and F. Caruso, *J. Am. Chem. Soc.* (in press).
49. J. Cho, K. Char, H.-D. Hong, and K.-B. Lee, *Adv. Mater*., **13**, 1076 (2001).
50. T. J. Rehg and B. G. Higgins, *Phys. Fluids*, **31**, 1360 (1998).
51. S. Middleman, *J. Appl. Phys*., **62**, 2530 (1987).
52. F. Ma and J. H. Hwang, *J. Appl. Phys.,* **68**, 1265 (1990).
53. S. S. Shiratori and M. F. Rubner, *Macromolecules*, **33**, 4213 (2000).
54. J. Schmitt, G. Decher, W. J. Dressick, S. L. Brandow, R. E. Geer, R. Shashidhar, and J. M. Calvert, *Adv. Mater.,* **9**, 61 (1997).
55. H. Hong, R. Steitz, S. Kirstein, and D. Davidov, *Adv. Mater.,* **10**, 1104 (1998).
56. M. Gao, B. Richter, S. Kirstein, and H. Mohwald, *J. Phys. Chem*., **102**, 4096 (1998).
57. H. Jang, S. Kim, and K. Char, *Langmuir*, **19**, 3094 (2003).
58. J. Cho, H. Jang, B. Yeom, H. Kim, R. Kim, S. Kim, K. Char, and F. Caruso, *Langmuir*, **22**, 1356 (2006).
59. I. A. Aksay, M. Trau, S. Manne, I. Honma, N. Yao, L. Zhou, P. Fenter, P. M. Eisenberg, and S. M. Gruner, *Science,* **273**, 892 (1996).
60. A. Sellinger, P. M. Weiss, A. Nguyen, Y. Lu, R. A. Assink, W. Gong, and C. J. Brinker, *Nature*, **394**, 256 (1998).
61. Z. Tang, N. Kotov, S. Magonov, and B. Ozturk, *Nature Materials*, **2**, 413 (2003).
62. B. Yeom, S. Kim, J. Cho, J. Hahn, and K. Char. *J. Adhesion*., **82**, 447 (2006).
63. Inorganic low molecular weight precursors were synthesized by the well-known sol-gel method. 10 g of TEOS was vigorously stirred with 3.42 g of H_2O and 0.05 g of HCl. After the formation of transparent TEOS sol (T-Sol), it was diluted with ethanol (weight ratio of TEOS : ethanol (EtOH) = 3 : 7).). In order to increase the electrostatic interfacial adhesion between the organic and the inorganic layer, 3-APTES was also added during the synthesis of TEOS sol (1.2 g of 3-APTES and 4.5 g of TEOS were injected to 23.7 g of EtOH) and then 1.42 g of H_2O and 0.6 g of HCl were slowly dropped into the mixture. After overnight reaction, a clear sol of the reaction product (A-Sol) was obtained.